

Simultaneously and Selectively Imaging a Cytoplasm Membrane and Mitochondria Using a Dual-Colored Aggregation-Induced Emission Probe

Yue Zheng,[§] Yiwen Ding,[§] Jiajun Ren, Yu Xiang, Zhigang Shuai,* and Aijun Tong*



Cite This: *Anal. Chem.* 2020, 92, 14494–14500



Read Online

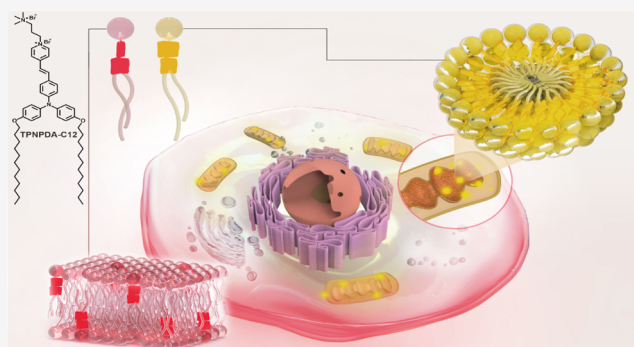
ACCESS |

Metrics & More

Article Recommendations

Supporting Information

ABSTRACT: Analysis of subcellular organelles (e.g., a cytoplasm membrane and mitochondria) during cellular processes can provide particularly useful information for our understanding of cell chemistry and biology. For this purpose, fluorescent probes capable of dynamically imaging multiple organelles in a simultaneous and selective manner are highly demanded, yet such probes are scarcely reported due to the challenges in molecular design. In this study, we developed a dual-colored aggregation-induced emission (AIE) probe TPNPDA-C12 with twisted intramolecular charge transfer (TICT) to visualize the membrane and mitochondria of the same cells through distinct fluorescence channels simultaneously. We also successfully used the probe to monitor and distinguish the dynamic changes of the organelles during cell apoptosis and necrosis induced by reactive oxygen species (ROS) and cytotoxins.



A cytoplasm membrane and mitochondria, serving as two important organelles ubiquitous in almost all eukaryotic cells, play critical roles in many cellular processes.^{1,2} A dynamic cooperation between the two organelles has been commonly observed, such as a mitochondria–plasma membrane tethering complex in mitochondria fission, partitioning, and inheritance,^{3–5} as well as active transport of substances between them in endocytosis.^{6,7} The cell membrane and mitochondria also undergo significant changes in the morphology and physical properties during cell apoptosis and necrosis.^{8–11} After severe injury causing necrosis, cells swell and the cytoplasm membrane becomes leaky and disrupted, allowing exchange of substances with the surrounding environment.^{12,13} On the other hand, mitochondria experience depolarization of mitochondrial membrane potential (MMP) and generate abnormal reactive oxygen species (ROS) levels associated with diseases including atherosclerosis, Alzheimer's disease, Parkinson's disease, and neuronal death.^{2,14,15} Therefore, visualizing the morphology and function changes of the cytoplasm membrane and mitochondria, preferably in a simultaneous and selective manner, is of crucial usefulness for research related to cell chemistry and biology.

Among numerous analytical techniques, fluorescence imaging has been recognized as one of the most powerful tools for live cell studies due to the high sensitivity and in situ observation, real-time monitoring, noninvasive measurement, and cost-effective performance.¹⁶ In recent years, fluorophores with aggregation-induced emission (AIE)^{17,18} characteristics

are emerging tools for chemical sensing and biological imaging due to their high sensitivity, excellent photostability, and biocompatibility. Benefiting from the strong fluorescence in their aggregate states and brighter emission at higher concentrations, organelle-specific AIE probes for imaging the cytoplasm membrane, mitochondria, lysosome, and nucleus have achieved promising progress.^{19–23} However, to date, most AIE probes are still monochromatic fluorescence emitting probes, and can only image a single organelle.

Dual-colored fluorescent probes²⁴ in bioimaging have attracted great interest for their advantages in simultaneously and dynamically imaging more than one subcellular organelles with a large contrast ratio. Most dual-colored fluorescent probes light up the target organelle in two fluorescence channels at different times through the migration of probe molecules, owing to the cellular environment variation.^{25–29} Only a few dual-colored probes have been reported to simultaneously image two different organelles in two different fluorescence channels,^{30,31} but unfortunately none of them can dynamically respond to external stimuli applied to the cells by a fluorescence switch, making the probes unsuitable for

Received: June 17, 2020

Accepted: September 17, 2020

Published: September 17, 2020



ACS Publications

© 2020 American Chemical Society

14494

<https://dx.doi.org/10.1021/acs.analchem.0c02596>
Anal. Chem. 2020, 92, 14494–14500

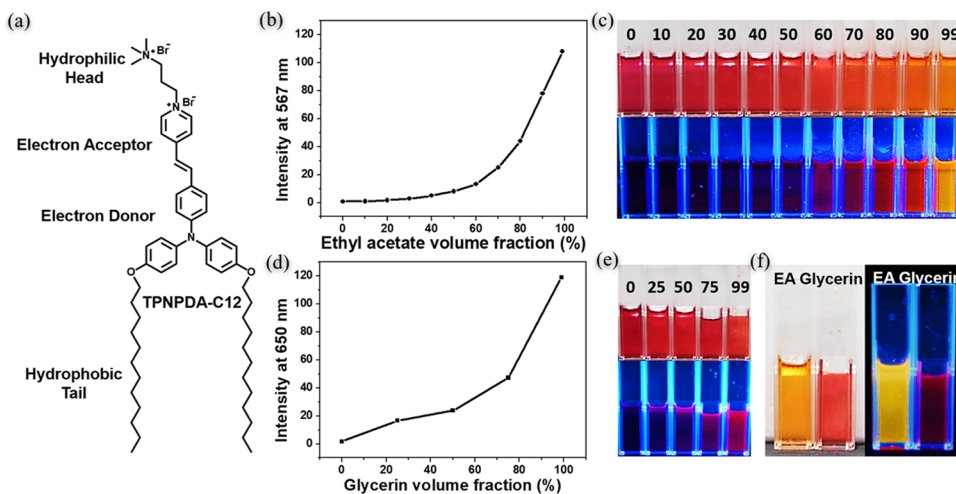


Figure 1. (a) Chemical structure and the design principle of TPNPDA-C12. (b) Fluorescence intensity of 100 μ M TPNPDA-C12 at 567 nm with different ethyl acetate/ethanol volume fractions. $\lambda_{\text{ex}} = 373$ nm. (c) Photographs of 100 μ M TPNPDA-C12 solution with different ethyl acetate/ethanol volume fractions under room light (top) or UV (bottom). (d) Fluorescence intensity of 100 μ M TPNPDA-C12 at 650 nm with different glycerin/ethanol volume fractions. $\lambda_{\text{ex}} = 500$ nm. (e) Photographs of 100 μ M TPNPDA-C12 solution with different glycerin/ethanol volume fractions under room light (top) or UV (bottom). (f) Photographs of 100 μ M TPNPDA-C12 solution with 99% ethyl acetate or glycerin under room light (left) or UV (right). Fluorescence pictures were taken under a 365 nm UV lamp.

tracking cellular processes. A handful of dual-colored fluorescent probes have been developed for the nucleus and mitochondria through a difference in charge interactions,^{25,26,31,32} as well as lysosomes and lipid droplets³⁰ via their distinct physiological environment. Nevertheless, no dual-colored fluorescent probe for simultaneously imaging the cell membrane and mitochondria is available so far.

To address the challenges, in this work, we designed and synthesized an amphiphilic and positively charged AIE probe, TPNPDA-C12 (Figure 1a), to image the cytoplasm membrane and mitochondria simultaneously and selectively. Our design of a TPNPDA-C12 molecule was based on three desired properties: (1) amphiphilicity with a critical micelle concentration (CMC) suitable for cell membrane binding^{19–21,33} along with positive charges for mitochondria targeting;³⁴ (2) a combined AIE and twisted intramolecular charge transfer (TICT)^{35–41} mechanism to allow fluorescence color changes in response to different environments in the two organelles upon stimuli; (3) biocompatibility and photostability to monitor the cell processes.²³

EXPERIMENTAL SECTION

Analytical Procedures. The stock solution (10 mM) of TPNPDA-C1, TPNPDA-C12, TPNPDA-C15, and TPNPDA-C18 were prepared in ethanol. In a typical detection, 30 μ L of stock solutions was added into a test tube, which was diluted to 2.97 mL of ethanol/ethyl acetate (or glycerin or 1× Dulbecco's phosphate buffered-saline (DPBS) buffer) to get final solutions with different ethyl acetate (or glycerin) fractions from 0 to 99% and the fluorescence spectra were recorded. For TPNPDA-C12, the photograph, UV absorption, and fluorescence spectra of the solutions in different solvents at 100 μ M were recorded.

Living Cell Staining and Imaging. Cells were grown in a 35 mm Petri dish with a coverslip at 37 °C. Modified staining procedures of TPNPDA-C1, TPNPDA-C12, TPNPDA-C15, and TPNPDA-C18 for most living cell imaging experiments are as follows. Stock solutions (1 mM) of the probes in ethanol were prepared. After that, 10 μ L of stock solution was added in

1 mL cultured adherent cells (HeLa, HepG2, or MCF-7) to get a final staining dye concentration at 10 μ M. The cells were incubated with the probe at 37 °C. After 10 min, cells were washed three times by 1× DPBS buffer, then 1 mL of a culture medium (Dulbecco's modified Eagle's medium (DMEM) containing 10% fetal bovine serum (FBS)) was added again for living cell imaging. Fluorescent images of the yellow channel were excited by 405 nm laser and collected at 490–560 nm, and the red channel was excited by 488 nm laser and collected at 600–700 nm.

Colocalization Experiments. Hela cells were stained by TPNPDA-C12 with a modified staining method and commercial subcellular organelle probes with a standard staining manual. The detailed experimental procedure is provided in the Supporting Information (SI).

Dynamic Imaging for Apoptosis and Necrosis Induced by ROS (H_2O_2) or Cytotoxin (STS). HeLa cells were first stained by TPNPDA-C12 with a modified staining method mentioned above. Five microliters of 3% H_2O_2 or 10 μ L of 1 mg/mL STS-DMSO stock solution was added and used with a CLSM's time mode for taking pictures every 2 min for a total of 30 min.

Other experimental details, including materials and instrumentation, synthesis method, calculation, cell culture, cytotoxicity, fluorescence lifetime imaging, and detailed colocalization experiments, are provided in the SI.

RESULTS AND DISCUSSION

Dual-Color Photoluminescence Property Study. As we expected, TPNPDA-C12 exhibited clear AIE characteristics in a cosolvent solution composed of ethyl acetate (poor solvent) and ethanol (good solvent), emitting fluorescence only in the presence of $\geq 60\%$ ethyl acetate (Figures 1b,c, and S1). Interestingly, unlike traditional AIE fluorophores, TPNPDA-C12 had dual-colored fluorescence that changed from red to yellow ($\lambda_{\text{max}} = 567$ nm, quantum yield (QY) = 2.2%) when the ethyl acetate fraction increased from 60 to 99%. The red fluorescence (Figure 1d,e) was also observed in a glycerin solution with minimal ethanol ($\lambda_{\text{max}} = 650$ nm, QY = 3.2%), as

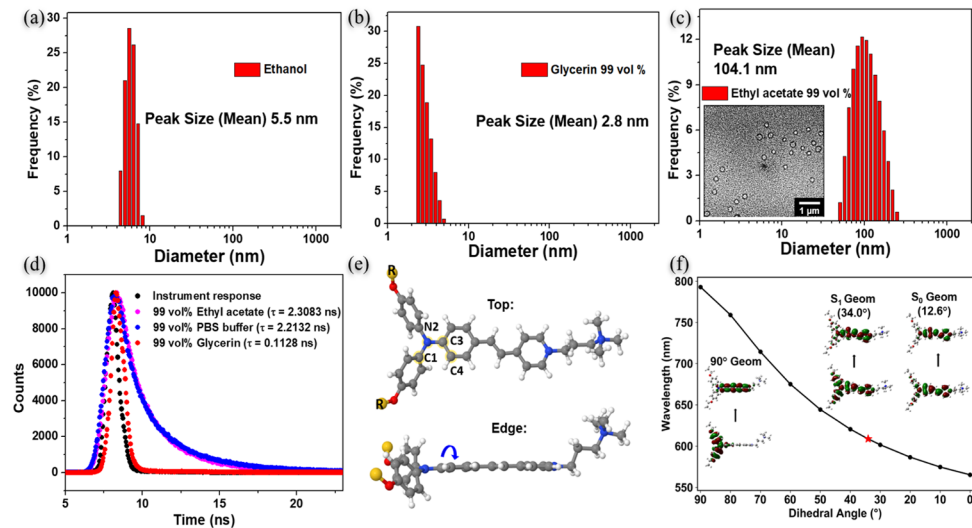


Figure 2. (a) Dynamic light scattering (DLS) analysis for $100 \mu\text{M}$ TPNPDA-C12 in (a) ethanol, (b) 99 vol % glycerin, and (c) 99 vol % ethyl acetate. Inset: the particle size of $100 \mu\text{M}$ TPNPDA-C12 in 99 vol % ethyl acetate measured by TEM. (d) Fluorescence decay curve and lifetime of $100 \mu\text{M}$ TPNPDA-C12 in 99 vol % ethyl acetate (pink), 99 vol % PBS buffer (blue), and 99 vol % glycerin (red). (e) Top view and the edge view of the optimized molecular geometry at an S_0 state. R represents the C12 alkyl chain. (f) Emission wavelength with different C1–N2–C3–C4 dihedral angles (the red star represents the fully relaxed S_1 geometry). Inset: the first pair of natural transition orbitals (NTO) at a D–A perpendicular geometry (left), optimized S_1 geometry (middle), and S_0 geometry (right). The NTO weights are all larger than 96%.

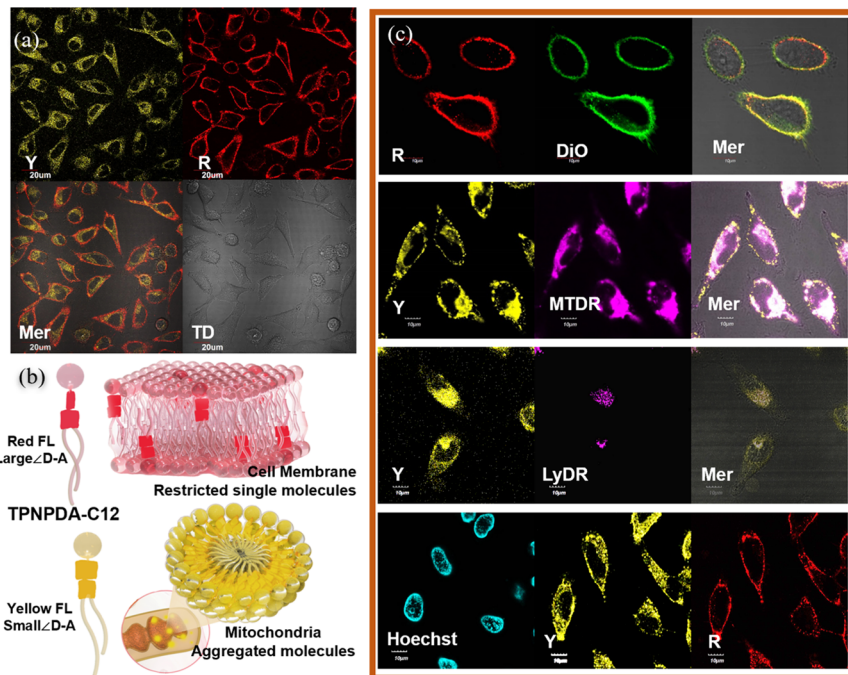


Figure 3. (a) Confocal fluorescence images of HeLa cells stained with TPNPDA-C12. Y: yellow channel (excited by 405 nm laser and collected at 490–560 nm), R: red channel (excited by 488 nm laser and collected at 600–700 nm), Mer: merged channel, TD: bright field. Scale bar is $20 \mu\text{m}$. (b) Schematic of TPNPDA-C12 for simultaneously dual-color imaging the cell membrane and mitochondria. (c) Confocal fluorescence images of HeLa cells for colocalization of TPNPDA-C12 with DiO, MTDR, LyDR, and Hoechst. Scale bar is $10 \mu\text{m}$.

well as an ethanol solution under a low temperature 77 K in liquid nitrogen (Figure S2). Dynamic light scattering (DLS) analysis of the solutions (Figure 2a–c) indicated the formation of molecular aggregates in 99% ethyl acetate (also found as ~ 100 nm spherical particles under transmission electron microscopy (TEM) after staining) but neither in ethanol nor in 99% glycerin (< 6 nm as a solvent background). These results suggested that the emissions in yellow and red were ascribed to the molecular aggregates and restricted monomers

of TPNPDA-C12, respectively. The yellow fluorescence has a longer lifetime (2.3 ns) than that of the red (0.11 ns, Figure 2d), in accordance with the general lifetimes for aggregates.^{18,22} The UV absorption spectra of TPNPDA-C12 in different solvents underwent a red shift with increasing solvent polarity, supporting the role of TICT in the fluorescence color change (Figures S3 and S4). Therefore, we concluded the dual-colored fluorescence of TPNPDA-C12 as a result of both AIE and TICT effects.

The microscopic mechanism of the dual-colored fluorescence is investigated with ab initio quantum chemistry calculations (see SI for the computational details). As the key dihedral angle $\angle C1-N2-C3-C4$ (Figure 2e) between the donor and the acceptor changes from a perpendicular geometry through a fully relaxed twisted S_1 geometry to a planar geometry (close to the S_0 state), the emission wavelength is blue-shifted monotonically, which is mainly due to the change of the excitation character from a pure intramolecular charge transfer state to a mixed local excitation/charge transfer state and finally a local excitation dominant state, as shown in Figure 2f. Therefore, because of the well-known aggregation-induced restriction of an intramolecular rotation effect,^{18,42} the D–A dihedral angle in the aggregate is close to that of the near planar S_0 geometry, giving a blue shift emission. In addition to the difference in excitation characters of the aggregate as described above, a previous computational work first coined “aggregation-induced blue-shifted emission” due to the reduced relaxation energy of the excited state in the aggregate,⁴³ which was found to be general for AIE chromophores and not specifically for the D–A molecule in this work. We believe these two effects both contributed to the blue-shifted emission of TPNPDA-C12 in its molecular aggregates.

For the amphiphilicity of TPNPDA-C12, we measured its critical micelle concentration (CMC) in an aqueous PBS buffer for its potential in staining the cytoplasm membrane. The CMC was calculated based on the curve of the fluorescence intensity depending on the concentration of TPNPDA-C12 in PBS (Figure S5a). The intersection of the two tangent lines gave a CMC value of about 45 μM , which was also confirmed by DLS analysis of the samples (Figure S5b), showing the presence of particles with the average diameter of 80.5 nm only at concentrations above 45 μM TPNPDA-C12. The CMC value and micelle size of TPNPDA-C12 in PBS were indeed appropriate for cellular studies. Besides, the fluorescence of TPNPDA-C12 remained unchanged under a pH range of 4.45–9.07 (Figure S5c), indicating its stability in live-cell imaging. On the other hand, we found low cytotoxicity of TPNPDA-C12 even at concentrations as high as 20 μM for various cell lines (Figures S8 and S9).

Simultaneous and Selective Live-Cell Imaging. Under a confocal laser scanning microscope (CLSM), we were very excited to observe a yellow fluorescence in the cytoplasm (490–560 nm emission channel excited by 405 nm laser) and a red fluorescence in the cell membrane (600–700 nm emission channel by 488 nm laser) in HeLa cells simultaneously using TPNPDA-C12 as the sole probe at 10 μM (Figure 3a). Based on the dual-colored fluorescence of TPNPDA-C12 showing yellow for molecular aggregates and red for restricted monomers (Figures 1f and S10), we assumed TPNPDA-C12 fused into the phospholipid bilayer of the cell membrane as monomers because of its much higher CMC over phospholipids. The red fluorescence in the cell membrane could also be explained by the high viscosity of the phospholipid bilayer, similar to glycerin (Figure 3b). In contrast, to our surprise, aggregation of TPNPDA-C12 occurred in the cytoplasm according to the yellow fluorescence inside the cells, though the concentration of TPNPDA-C12 used in cell culture was much lower than its CMC. Fluorescence lifetime imaging microscope (FLIM) measurement confirmed the presence of restricted monomers in the cell membrane and molecular aggregates in the cytoplasm by

the characteristic lifetimes (Figure S11). Therefore, we believe there must be an intracellular microenvironment accumulating the probe to high local concentrations to form the TPNPDA-C12 aggregates. To pinpoint the exact location of TPNPDA-C12 in subcellular organelles, we performed colocalization experiments using commercially available probes known for specific subcellular organelles. As shown in Figures 3c and S14, Pearson’s coefficient of each commercial dye was calculated by the colocalization scatter plots. The red fluorescence of TPNPDA-C12 was found nicely colocalized with the cytoplasm membrane dye DiO (coefficient as high as 0.85). The yellow fluorescence of TPNPDA-C12, on the other hand, overlapped finely with the mitochondria dye MTDR (coefficient as high as 0.86), and almost without apparent correlation with the lysosome dye LyDR (coefficient as only 0.44, similar to MTG and LyDR as 0.35, Figure S15). Besides, for the endoplasmic reticulum (ER) and the Golgi apparatus, the yellow fluorescence also exhibits little correlation (Figure S16, coefficient as only 0.51 and 0.54, respectively), similar to the coefficient of commercial mitotracker green (MTG) with the ER and the Golgi apparatus (0.48 and 0.46, respectively, Figure S17). These results indicated that TPNPDA-C12 was simultaneously distributed in the cell membrane and mitochondria inside live HeLa cells, with a selective dual-colored fluorescence in red and yellow, respectively. Besides HeLa cells, we also studied the behaviors of TPNPDA-C12 in HepG2 and MCF-7 cells and found their localization of red and yellow fluorescence was the same, suggesting its general use regardless of cell lines (Figure S18).

Effect of the Alkyl Chain Length on Subcellular Localization. The length of an alkyl chain usually affected the CMC and solubility of amphiphilic molecules.⁴⁴ In addition to TPNPDA-C12, we synthesized its analogues with alkyl chains in the length of 1, 15, and 18 carbons (named as TPNPDA-C1, TPNPDA-C15, and TPNPDA-C18, respectively). They had almost the same fluorescence properties in poor solvents as well as in glycerin compared with TPNPDA-C12 (Figures S19–21), since they shared the same AIE and TICT characteristics of the identical core fluorophore. However, when applied for living cell imaging on HeLa cells, TPNPDA-C1, TPNPDA-C12, TPNPDA-C15, and TPNPDA-C18 displayed a dramatic difference in intracellular localizations. As shown in Figure 4, TPNPDA-C15 with a longer alkyl chain than TPNPDA-C12 could only stain the cell membrane in red while giving no yellow fluorescence in the cytoplasm, probably due to its stronger amphiphilicity blocking its entry into an intracellular environment. Colocalization experiments show that the colocalization coefficient of TPNPDA-C15 with DiO reached a high value of 0.92 (Figure S23). TPNPDA-C18 was unable to stain the cells at all, likely because it had an ultralow CMC and formed large aggregates in a medium with little cellular uptake. When the alkyl chain was reduced to only one carbon, TPNPDA-C1 initially showed a similar pattern in imaging HeLa cells as TPNPDA-C12, but the red fluorescence in the cell membrane was not stable for TPNPDA-C1 and gradually diffused over time, indicating the critical role of sufficient amphiphilicity in probe design (Figure S22).²¹

Dynamically Imaging and Distinguishing Apoptosis and Necrosis. Taking advantage of its dual-colored fluorescence for simultaneously imaging the cytoplasm membrane and mitochondria in red and yellow emission channels, respectively, TPNPDA-C12 could serve as an ideal probe for dynamically imaging cell processes. Here, we applied

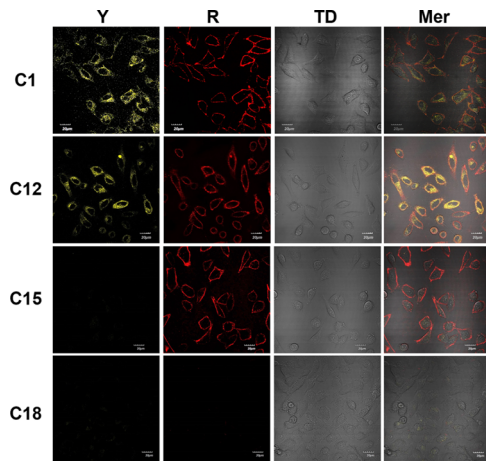


Figure 4. Confocal fluorescence images of HeLa cells stained with TPNPDA-C1, TPNPDA-C12, TPNPDA-C15, and TPNPDA-C18 by the modified staining method ($10 \mu\text{M}$ probes incubated for 10 min). Scale bar is $20 \mu\text{m}$.

TPNPDA-C12 to monitor the cytoplasm membrane and mitochondria during apoptosis and necrosis, the important ways of cell death.^{8,11,45,46} Many research studies have been reported with a variety of fluorescent probes for ratiometrically^{26,47} or dynamically^{25,48,49} imaging apoptotic and necrotic processes.²⁴ However, no probe is reported yet to study the roles of multiple subcellular organelles in apoptosis and necrosis. We introduced high concentration of hydrogen peroxide (H_2O_2) as ROS stimulation to induce rapid cell apoptosis and necrosis.^{9,10,45,50} ROS-induced apoptosis and necrosis destroyed the integrity of the cell membrane, and dead cells could be identified by staining with propidium iodide (PI) that only entered the cells after the rupture of the cell membrane.^{12,13} As shown in Figure 5a and Movie S1, after adding $5 \text{ mM H}_2\text{O}_2$ in HeLa cells stained by TPNPDA-C12, the yellow fluorescence in mitochondria almost remained constant, while the red fluorescence in the cell membrane gradually weakened over time and disappeared within 30 min.

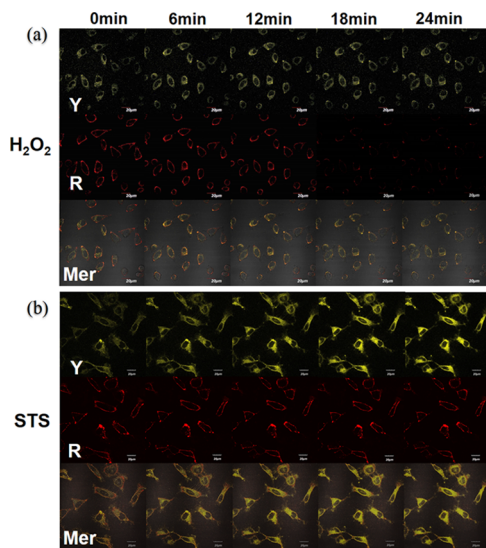


Figure 5. Confocal fluorescence images of HeLa cells prestained with TPNPDA-C12 (a) treated with $5 \text{ mM H}_2\text{O}_2$ for 30 min and (b) treated with $10 \mu\text{M}$ STS for 30 min. Scale bar is $20 \mu\text{m}$.

This result indicated that ROS-induced apoptosis and necrosis started with relatively fast destruction of the cell membrane when mitochondria in the cytoplasm were not damaged yet. On the other hand, we used staurosporine (STS), a commonly used chemical drug for cytotoxin-induced apoptosis and necrosis, to see its difference from ROS-induced cell death. Interestingly, in 30 min after addition of $10 \mu\text{M}$ STS, the yellow fluorescence enhanced significantly and the red fluorescence remained almost unchanged (Figure 5b and Movie S3). Since it was difficult to intuitively determine through the images whether the cells were already in the apoptotic phase after 30 min incubation with STS, we used flow cytometry to quantitatively characterize the cell viability. HeLa cells were preincubated with $10 \mu\text{M}$ STS or equal DMSO as a control and then treated by the apoptosis assay kit of annexin V–allophycocyanin (APC)/PI double staining. As shown in Figure S24a, the fluorescence of neither APC nor PI was detected in HeLa cells incubated without STS (UL = 0.51%, UR = 2.93%) and live cell remained 95.72% (LL). For the sample after STS treatment for 30 min, 56.95% of the cells were stained by annexin V–APC (UL), indicating these cells were in an apoptotic phase (Figure S24b). It was also found that 39.62% of the cells were stained by both annexin V–APC and PI (UR) that had already died of necrosis. Based on these results, we speculated that STS as a competitive inhibitor of protein kinases through the prevention of ATP binding to the kinase⁵¹ acted on mitochondria and inactivated protein kinases there. The damage caused in mitochondria might increase mitochondria membrane permeability and allow dispersed TPNPDA-C12 molecules in the cytoplasm to accumulate into mitochondria and form aggregates to enhance the yellow fluorescence. During this process, the integrity of the cell membrane was not compromised, so the red fluorescence was not affected.

CONCLUSIONS

In conclusion, we designed and synthesized an amphiphilic AIE probe TPNPDA-C12, which could simultaneously and selectively image a cell membrane and mitochondria in a dual-colored mode. Through charge interaction, TPNPDA-C12 accumulated in mitochondria to form molecular aggregates displaying a yellow fluorescence. On the other hand, TPNPDA-C12 fused into the cytoplasm membrane by amphiphilic interaction and the restricted monomers there showed a red fluorescence. The alkyl chain length of TPNPDA analogues determined their distribution in the subcellular organelles. We also successfully used TPNPDA-C12 to dynamically visualize the cell membrane and mitochondria during distinct ROS- and cytotoxin-induced cell apoptosis and necrosis. Because of its advantages in dual-colored fluorescence, low cytotoxicity, and simultaneous and selective imaging of the cytoplasm membrane and the mitochondria, we believe TPNPDA-C12 is a promising probe to study live cell processes for cell biology and disease mechanisms.

ASSOCIATED CONTENT

Supporting Information

The Supporting Information is available free of charge at <https://pubs.acs.org/doi/10.1021/acs.analchem.0c02596>.

Materials and instruments, the synthesis method and experimental procedures, UV and FL spectra, confocal fluorescent images, flow cytometric analysis, and

characterizations of the synthesized compounds (NMR, ESI-MS) ([PDF](#))

TPNPDA-C12-stained HeLa cells after adding 5 μ L of a 3 wt % H₂O₂ solution in water recording for 30 min ([AVI](#))

TPNPDA-C12-stained HeLa cells after adding 5 μ L of water recording for 30 min ([AVI](#))

TPNPDA-C12-stained HeLa cells after adding 10 μ L of a 1 mg/mL STS solution in DMSO recording for 30 min ([AVI](#))

TPNPDA-C12-stained HeLa cells after adding 10 μ L of DMSO recording for 30 min ([AVI](#))

AUTHOR INFORMATION

Corresponding Authors

Zhigang Shuai — Department of Chemistry, Key Laboratory of Organic Optoelectronics and Molecular Engineering (Ministry of Education), Tsinghua University, Beijing 100084, P. R. China; [orcid.org/0000-0003-3867-2331](#); Email: zgshuai@mail.tsinghua.edu.cn

Aijun Tong — Department of Chemistry, Beijing Key Laboratory for Microanalytical Methods and Instrumentation, Key Laboratory of Bioorganic Phosphorus Chemistry and Chemical Biology (Ministry of Education), Tsinghua University, Beijing 100084, P. R. China; [orcid.org/0000-0003-0633-4098](#); Email: tongaj@mail.tsinghua.edu.cn

Authors

Yue Zheng — Department of Chemistry, Beijing Key Laboratory for Microanalytical Methods and Instrumentation, Key Laboratory of Bioorganic Phosphorus Chemistry and Chemical Biology (Ministry of Education), Tsinghua University, Beijing 100084, P. R. China

Yiwen Ding — Department of Chemistry, Beijing Key Laboratory for Microanalytical Methods and Instrumentation, Key Laboratory of Bioorganic Phosphorus Chemistry and Chemical Biology (Ministry of Education), Tsinghua University, Beijing 100084, P. R. China

Jiajun Ren — Department of Chemistry, Key Laboratory of Organic Optoelectronics and Molecular Engineering (Ministry of Education), Tsinghua University, Beijing 100084, P. R. China; [orcid.org/0000-0002-1508-4943](#)

Yu Xiang — Department of Chemistry, Beijing Key Laboratory for Microanalytical Methods and Instrumentation, Key Laboratory of Bioorganic Phosphorus Chemistry and Chemical Biology (Ministry of Education), Tsinghua University, Beijing 100084, P. R. China

Complete contact information is available at:

<https://pubs.acs.org/10.1021/acs.analchem.0c02596>

Author Contributions

Y.Z. and Y.D. contributed equally in probe design and synthesis, characterization, and live-cell imaging. All authors have given approval to the final version of the paper. Dr. J.R. and Prof. Z.S. contributed in theoretical calculation and analysis. Associate Prof. Y.X. contributed to paper writing instruction and revision. Prof. A.T. contributed to all of the works except for theoretical calculation and analysis.

Funding

This work is supported by the National Natural Science Foundation of China (Nos. 21775084, 21788102, 21974076, and 21621003).

Notes

The authors declare no competing financial interest.

ACKNOWLEDGMENTS

We gratefully appreciate Xudong Wu (Department of Chemistry, Tsinghua University) for his valuable advice and guidance on molecular design and organic synthesis. We would like to sincerely acknowledge the assistance of the Imaging Core Facility, Technology Center for Protein Science, Tsinghua University for the assistance of using FV 1200 CLSM and FLIM-FCS, especially Yanli Zhang for her enthusiastic and professional guidance in cell imaging technology. We thank Pengcheng Jiao (Center of Biomedical Analysis, Tsinghua University) for his kind help of flow cytometry analysis.

ABBREVIATIONS USED

AIE	aggregation-induced emission
ACQ	aggregation-caused quenching
TICT	twisted intramolecular charge transfer
ROS	reactive oxygen species
MMP	mitochondria membrane potential
CMC	critical micelle concentration
NTO	natural transition orbitals
LE	local excitation
CT	charge transfer
CLSM	confocal laser scanning microscope
FLIM	fluorescence lifetime imaging microscope
DLS	dynamic light scattering
TEM	transmission electron microscopy
STS	staurosporine

REFERENCES

- (1) Mueller, P.; Rudin, D. O.; Ti Tien, H.; Wescott, W. C. *Nature* **1962**, *194*, 979–980.
- (2) Green, D. R.; Reed, J. C. *Science* **1998**, *281*, 1309–1312.
- (3) Cerveny, K. L.; Studer, S. L.; Jensen, R. E.; Sesaki, H. *Dev. Cell* **2007**, *12*, 363–375.
- (4) Lackner, L. L.; Ping, H.; Graef, M.; Murley, A.; Nunnari, J. *Proc. Natl. Acad. Sci. U.S.A.* **2013**, *110*, E458–E467.
- (5) Westermann, B. *Curr. Opin. Cell Biol.* **2015**, *35*, 1–6.
- (6) Doherty, G. J.; McMahon, H. T. *Annu. Rev. Biochem.* **2009**, *78*, 857–902.
- (7) Wei, Z.; Su, W.; Lou, H.; Duan, S.; Chen, G. *J. Mol. Cell Biol.* **2018**, *10*, 539–548.
- (8) Smith, C. A.; Williams, G. T.; Kingston, R.; Jenkinson, E. J.; Owen, J. J. T. *Nature* **1989**, *338*, 10.
- (9) Peter, M. E. *Nature* **2011**, *471*, 310–312.
- (10) Vaux, D. L.; Korsmeyer, S. J. *Cell* **1999**, *96*, 245–254.
- (11) Narayan, N.; Lee, I. H.; Borenstein, R.; Sun, J.; Wong, R.; Tong, G.; Fergusson, M. M.; Liu, J.; Rovira, I. I.; Cheng, H.-L.; Wang, G.; Gucek, M.; Lombard, D.; Alt, F. W.; Sack, M. N.; Murphy, E.; Cao, L.; Finkel, T. *Nature* **2012**, *492*, 199–204.
- (12) Alberts, B. J. A.; Lewis, J.; Raff, M.; Roberts, K.; Walter, P. *Molecular Biology of the Cell*, 4th ed.; Garland Science: New York, 2002.
- (13) Lodish, H. B. A.; Kaiser, C. A.; Krieger, M.; Bretscher, A.; Ploegh, H.; Amon, A.; Scott, M. P. *Molecular Cell Biology*, 7th ed.; Scientific American Books: New York, 1987.
- (14) Evan, G. I.; Vousden, K. H. *Nature* **2001**, *411*, 342–348.
- (15) Sheu, S.-S.; Nauduri, D.; Anders, M. W. *Biochim. Biophys. Acta, Mol. Basis Dis.* **2006**, *1762*, 256–265.
- (16) Borisov, S. M.; Wolfbeis, O. S. *Chem. Rev.* **2008**, *108*, 423–461.
- (17) Hong, Y.; Lam, J. W. Y.; Tang, B. Z. *Chem. Soc. Rev.* **2011**, *40*, 5361–5388.

- (18) Mei, J.; Leung, N. L. C.; Kwok, R. T. K.; Lam, J. W. Y.; Tang, B. Z. *Chem. Rev.* **2015**, *115*, 11718–11940.
- (19) Li, Y.; Wu, Y.; Chang, J.; Chen, M.; Liu, R.; Li, F. *Chem. Commun.* **2013**, *49*, 11335–11337.
- (20) Zhang, W.; Huang, Y.; Chen, Y.; Zhao, E.; Hong, Y.; Chen, S.; Lam, J. W. Y.; Chen, Y.; Hou, J.; Tang, B. Z. *ACS Appl. Mater. Interfaces* **2019**, *11*, 10567–10577.
- (21) Hu, F.; Liu, B. *Org. Biomol. Chem.* **2016**, *14*, 9931–9944.
- (22) Peng, L.; Xu, S.; Zheng, X.; Cheng, X.; Zhang, R.; Liu, J.; Liu, B.; Tong, A. *Anal. Chem.* **2017**, *89*, 3162–3168.
- (23) Leung, C. W. T.; Hong, Y.; Chen, S.; Zhao, E.; Lam, J. W. Y.; Tang, B. Z. *J. Am. Chem. Soc.* **2013**, *135*, 62–65.
- (24) Tian, M.; Ma, Y.; Lin, W. *Acc. Chem. Res.* **2019**, *S2*, 2147–2157.
- (25) Tian, M.; Sun, J.; Dong, B.; Lin, W. *Angew. Chem., Int. Ed.* **2018**, *S7*, 16506–16510.
- (26) Tian, M.; Sun, J.; Dong, B.; Lin, W. *Anal. Chem.* **2019**, *91*, 10056–10063.
- (27) Zhao, N.; Li, Y.; Yang, W.; Zhuang, J.; Li, Y.; Li, N. *Chem. Sci.* **2019**, *10*, 9009–9016.
- (28) Park, S. J.; Juvekar, V.; Jo, J. H.; Kim, H. M. *Chem. Sci.* **2020**, *11*, 596–601.
- (29) Gao, Y.; He, Z.; He, X.; Zhang, H.; Weng, J.; Yang, X.; Meng, F.; Luo, L.; Tang, B. Z. *J. Am. Chem. Soc.* **2019**, *141*, 20097–20106.
- (30) Zheng, X.; Zhu, W.; Ni, F.; Ai, H.; Gong, S.; Zhou, X.; Sessler, J. L.; Yang, C. *Chem. Sci.* **2019**, *10*, 2342–2348.
- (31) Chao, X.-J.; Wang, K.-N.; Sun, L.-L.; Cao, Q.; Ke, Z.-F.; Cao, D.-X.; Mao, Z.-W. *ACS Appl. Mater. Interfaces* **2018**, *10*, 13264–13273.
- (32) Zhao, Y.; Zhang, C.; Liu, J.; Li, D.; Tian, X.; Wang, A.; Li, S.; Wu, J.; Tian, Y. *J. Mater. Chem. B* **2019**, *7*, 3633–3638.
- (33) Wang, Z.; Zhou, F.; Wang, J.; Zhao, Z.; Qin, A.; Yu, Z.; Tang, B. Z. *Sci. China: Chem.* **2018**, *61*, 76–87.
- (34) Hoye, A. T.; Davoren, J. E.; Wipf, P.; Fink, M. P.; Kagan, V. E. *Acc. Chem. Res.* **2008**, *41*, 87–97.
- (35) Hu, R.; Lager, E.; Aguilera-Aguilar, A.; Liu, J.; Lam, J. W. Y.; Sung, H. H. Y.; Williams, I. D.; Zhong, Y.; Wong, K. S.; Pena-Cabrera, E.; Tang, B. Z. *J. Phys. Chem. C* **2009**, *113*, 15845–15853.
- (36) Grabowski, Z. R.; Rotkiewicz, K.; Rettig, W. *Chem. Rev.* **2003**, *103*, 3899–4032.
- (37) Sasaki, S.; Drummen, G. P. C.; Konishi, G.-i. *J. Mater. Chem. C* **2016**, *4*, 2731–2743.
- (38) Wang, D.; Su, H.; Kwok, R. T. K.; Hu, X.; Zou, H.; Luo, Q.; Lee, Michelle M. S.; Xu, W.; Lam, J. W. Y.; Tang, B. Z. *Chem. Sci.* **2018**, *9*, 3685–3693.
- (39) Wang, D.; Lee, M. M. S.; Shan, G.; Kwok, R. T. K.; Lam, J. W. Y.; Su, H.; Cai, Y.; Tang, B. Z. *Adv. Mater.* **2018**, *30*, No. 1802105.
- (40) Zheng, X.; Wang, D.; Xu, W.; Cao, S.; Peng, Q.; Tang, B. Z. *Mater. Horiz.* **2019**, *6*, 2016–2023.
- (41) He, X.; Situ, B.; Gao, M.; Guan, S.; He, B.; Ge, X.; Li, S.; Tao, M.; Zou, H.; Tang, B. Z.; Zheng, L. *Small* **2019**, *15*, No. 1905080.
- (42) Shuai, Z.; Peng, Q. *Natl. Sci. Rev.* **2017**, *4*, 224–239.
- (43) Wu, Q.; Zhang, T.; Peng, Q.; Wang, D.; Shuai, Z. *Phys.Chem.Chem.Phys.* **2014**, *16*, 5545–5552.
- (44) Tanford, C. *The Hydrophobic Effect*; John Wiley & Sons: New York, 1980.
- (45) Fritsch, M.; Günther, S. D.; Schwarzer, R.; Albert, M.-C.; Schorn, F.; Werthenbach, J. P.; Schiffmann, L. M.; Stair, N.; Stocks, H.; Seeger, J. M.; Lamkanfi, M.; Krönke, M.; Pasparakis, M.; Kashkar, H. *Nature* **2019**, *575*, 683–687.
- (46) Muzio, M.; Chinnaian, A. M.; Kischkel, F. C.; O'Rourke, K.; Shevchenko, A.; Ni, J.; Scaffidi, C.; Bretz, J. D.; Zhang, M.; Gentz, R.; Mann, M.; Krammer, P. H.; Peter, M. E.; Dixit, V. M. *Cell* **1996**, *85*, 817–827.
- (47) Shynkar, V. V.; Klymchenko, A. S.; Kunzelmann, C.; Duportail, G.; Muller, C. D.; Demchenko, A. P.; Freyssinet, J.-M.; Mely, Y. *J. Am. Chem. Soc.* **2007**, *129*, 2187–2193.
- (48) Martinić, I.; Eliseeva, S. V.; Nguyen, T. N.; Pecoraro, V. L.; Petoud, S. *J. Am. Chem. Soc.* **2017**, *139*, 8388–8391.
- (49) Hu, Q.; Gao, M.; Feng, G.; Chen, X.; Liu, B. *ACS Appl. Mater. Interfaces* **2015**, *7*, 4875–4882.
- (50) Cordeiro, M. F.; Guo, L.; Luong, V.; Harding, G.; Wang, W.; Jones, H. E.; Moss, S. E.; Sillito, A. M.; Fitzke, F. W. *Proc. Natl. Acad. Sci. U.S.A.* **2004**, *101*, 13352–13356.
- (51) Karaman, M. W.; Herrgard, S.; Treiber, D. K.; Gallant, P.; Atteridge, C. E.; Campbell, B. T.; Chan, K. W.; Ciceri, P.; Davis, M. I.; Edeen, P. T.; Faraoni, R.; Floyd, M.; Hunt, J. P.; Lockhart, D. J.; Milanov, Z. V.; Morrison, M. J.; Pallares, G.; Patel, H. K.; Pritchard, S.; Wodicka, L. M.; Zarrinkar, P. P. *Nat. Biotechnol.* **2008**, *26*, 127–132.